Attempts to Delineate the Relative Contributions of Changes in Hydrophobicity and Packing to Changes in Stability of Ribonuclease S Mutants†

Mili Das,‡ Bharathi Vasudeva Rao,‡ Sanjukta Ghosh,‡ and Raghavan Varadarajan*,‡,§

Molecular Biophysics Unit, Indian Institute of Science, Bangalore 560 012, India, and Chemical Biology Unit, Jawaharlal Center for Advanced Scientific Research, Jakkur, P. O., Bangalore 560 004, India

Received January 1, 2005; Revised Manuscript Received February 14, 2005

ABSTRACT: While the hydrophobic driving force is thought to be a major contributor to protein stability, it is difficult to experimentally dissect out its contribution to the overall free energy of folding. We have made large to small substitutions of buried hydrophobic residues at positions 8 and 13 in the peptide/protein complex, RNase-S, and have characterized the structures by X-ray crystallography. The thermodynamics of association of these mutant S peptides with S protein was measured in the presence of different concentrations of methanol and ethanol. The reduction in the strength of the hydrophobic driving force in the presence of these organic solvents was estimated from surface-tension data as well as from the dependence of the ΔC_p of protein/peptide binding on the alcohol concentration. The data indicated a decrease in the strength of the hydrophobic driving force of about 30−40% over a 0−30% range of the alcohol concentration. We observe that large to small substitutions destabilize the protein. However, the amount of destabilization, relative to the wild type, is independent of the alcohol concentration over the range of alcohol concentrations studied. The data clearly indicate that decreased stability of the mutants is primarily due to the loss of packing interactions rather than a reduced hydrophobic driving force and suggest a value of the hydrophobic driving force of less than 18 cal mol^{-1} Å^2.

It is generally believed that the hydrophobic driving force is a major determinant of protein stability (*1*). There are several other contributors to the overall free energy of folding ($\Delta G°_f$). These include differences in hydrogen bonding, van der Waals interactions, electrostatic interactions, and conformational entropy between the folded and unfolded states. Hence, it is difficult to estimate the contribution of the hydrophobic driving force alone to the overall $\Delta G°_f$. Many previous estimates have been derived from measurements of the thermodynamics of transfer of model compounds from the solid, vapor, or liquid phase into aqueous solution (*2*−*7*). An alternative approach taken to measure this contribution is detailed thermodynamic and structural studies of proteins having large to small substitutions of buried, nonpolar amino acid residues (*8*−*11*). Such substitutions should result in a decreased hydrophobic driving force for folding. Previous studies have used the difference in free energy of folding upon mutation, $\Delta\Delta G°_f$ [$\Delta\Delta G°_f = \Delta G°_f$(mutant) − $\Delta G°_f$(wild type)], to estimate the contribution of the hydrophobic driving force to protein folding. In addition to a reduced hydrophobic driving force, such mutations often result in formation of cavities in the interior of the protein (*11*−*14*), leading to a loss of van der Waals interactions. It was previously suggested (*15*) that loss of packing interactions, rather than a reduced hydrophobic driving force, largely determines the value of $\Delta\Delta G°_f$ for these cavity-containing mutants. To further clarify this issue, we have carried out a series of thermodynamic and structural studies in mutants of the protein/peptide complex, ribonuclease S (RNase S).[1]

Bovine pancreatic ribonuclease A (RNase-A) can be cleaved by subtilisin between residues 20 and 21 to yield two fragments, S peptide (residues 1−20) and S protein (residues 21−124) (*16*, *17*). These fragments can be separated and reconstituted to form the noncovalently associated S peptide/S protein complex, ribonuclease S (RNase-S), which is catalytically active and has a three-dimensional structure very similar to that of native RNase-A (*18*, *19*). Because residues 16−20 are not important for the binding of the two fragments (*20*), a truncated S peptide (S-pep) comprising of residues 1−15 can be used instead of the 20-residue peptide. The binding energetics of this association can be studied using isothermal titration calorimetry (ITC). This enables the study of mutational effects on the thermodynamic parameters of association at different temperatures in the absence of any denaturants. In addition, mutants can

† This work was funded by grants from the Wellcome Trust and Council for Scientific and Industrial Research, Government of India to R.V. M.D. is a Postdoctoral Fellow of the Department of Biotechnology, Government of India. R.V. is a recipient of the Swarnajayanthi Fellowship, Government of India, and a Senior Research Fellowship from the Wellcome Trust.

* To whom correspondence should be addressed: Molecular Biophysics Unit, Indian Institute of Science, Bangalore, 560 012, India. E-mail: varadar@mbu.iisc.ernet.in. Telephone: 91-80-22932612. Fax: 91-80-23600535.

‡ Indian Institute of Science.

§ Jawaharlal Center for Advanced Scientific Research.

[1] Abbreviations: RNase, ribonuclease; Nle, norleucine; Nva, norvaline, Anb, aminobutyric acid; TFA, trifluoroacetic acid; WT, wild type; CNS, crystallography and NMR system; NMR, nuclear magnetic resonance; rmsd, root-mean-square deviation; MC, Monte Carlo; CD, circular dichroism; S-pep, S-peptide; MALDI−MS, matrix-assisted laser desorption/ionization mass spectroscopy; ELISA, enzyme-linked immunosorbent assay; HPLC, high-pressure liquid chromatography.

10.1021/bi050001+ CCC: $30.25
Published on Web 03/19/2005

be readily crystallized and a variety of nonnatural amino acid mutants can be incorporated into the S peptide. Residues Phe8 and Met13 are two hydrophobic residues in S peptide that are buried in the interior of RNase-S. These residues are important for the binding of S peptide to S protein (*17*, *21*). These positions have been mutated to smaller, hydrophobic residues, and the impact on the thermodynamic parameters and structure of the enzyme have been reported previously (*13*, *15*, *22*−*24*). In the present study, we have incorporated additional substitutions at these two positions in the S-pep. The thermodynamics of association of these mutant S-pep's with S protein in the presence of different concentrations of methanol and ethanol was examined to characterize the effect of a reduced hydrophobic driving force on the binding energetics of this fragment complementation system. We have also solved the crystal structures of three of these mutant complexes and analyzed the change in cavity volumes as a result of the substitutions at positions 8 and 13.

MATERIALS AND METHODS

Materials. RNase-S was prepared from RNase-A (Sigma, Type XII A), by subtilisin cleavage (*16*) and as modified by Neumann and Hofsteenge (*25*). S protein was purified from RNase-S by reverse-phase HPLC on a C_{18} Vydac preparative column using a 5−95% acetonitrile gradient with 0.1% TFA. The S protein and S-pep eluted at 45 and 30% acetonitrile, respectively. These fractions were placed in a speedvac to remove the acetonitrile and then lyophilized. The purified S protein gave a single peak at the expected molecular weight of 11 527.8 (this corresponds to cleavage between the 20th and 21st residues) on a mass spectrometer. All traces of acetonitrile were removed by repeated lyophilization of the S protein and dissolution in water. The concentration of purified S protein was determined from the absorption of its aqueous solution at 280 nm [$\epsilon = 9.56\ \mathrm{mM^{-1}\ cm^{-1}}$ (*23*)]. The S-pep mutants M13Nle, M13Nva, M13Anb, F8NleM13-Nle, F8NvaM13Nle, and F8AnbM13Nle were obtained from the Keck Biotechnology Resource Laboratory at Yale University. Anb, Nva, and Nle are three nonnatural amino acids, aminobutyric acid, norvaline, and norleucine, and have the side chains $-CH_2-CH_3$, $-CH_2-CH_2-CH_3$, and $-CH_2-CH_2-CH_2-CH_3$, respectively. Because all peptides with mutations at position 8 contain the conservative M13Nle mutation, we hereafter refer to this as the wild type (WT) and the remaining mutants as 13Nva, 13Anb, 8Nle, 8Nva, and 8Anb, respectively. The crude peptides were purified by reverse-phase HPLC on a Vydac C_{18} preparative column using a water/acetonitrile gradient containing 0.1% TFA. The samples were repeatedly lyophilized to remove any traces of the solvent components. The presence of mutant S-pep in the peak fraction was confirmed by MALDI−MS. The concentration of the peptide stocks was calculated assuming that 70% of the weight of the lyophilized powder corresponds to the peptide. Concentrations calculated in this fashion agreed closely with values determined by quantitative amino acid analysis described previously (*23*, *24*). The purified S protein and the peptides were stored at −20 °C. Alternatively, the S protein was purified by gel-filtration chromatography through Sephadex G-50 equilibrated with 10% formic acid. Formic acid was then removed from the protein by repeated lyophilization.

ITC. S protein and S-pep solutions used for the titration experiments were prepared by redissolving the lyophilized samples in an appropriate volume of buffer. For 13Nva and 13Anb, 50 mM sodium acetate buffer at pH 6.0 containing 100 mM NaCl and different percentages (v/v) of organic solvent (methanol or ethanol) was used. For the S-pep mutants 8Nle, 8Nva, and 8Anb, 50 mM sodium phosphate buffer at pH 7.0 containing 100 mM NaCl and different percentages (v/v) of organic solvent (methanol or ethanol) was used for the titrations. Sodium phosphate is known to enhance binding (*15*) relative to sodium acetate. It was necessary to use the latter buffer for mutants at position 8 because these have intrinsically weaker affinity than similar mutants at position 13 (*15*, *24*). Nle was used in preference to the Met present in the native S-pep for two reasons. First, Met is prone to air oxidation. Second, conservative substitution of the Met sulfur atom with a methylene group leads to unexpectedly large values of $\Delta\Delta C_p$, $\Delta\Delta H°$, and $\Delta\Delta S$ (*15*, *22*). To avoid such complications in the interpretation of the thermodynamic data of large to small residue substitutions and because all of the peptides used in the study have the M13Nle substitution, the M13Nle peptide serves as the reference (WT) peptide for the purpose of our study. With this choice of reference peptide, values of $\Delta\Delta C_p$ have previously been shown to be close to zero (*15*). Hence, values of $\Delta\Delta H°$, $\Delta\Delta S$, and $\Delta\Delta G°$ are temperature-independent, facilitating interpretation of the results. Reference titrations of WT binding to S protein were performed in both buffers as a function of methanol and ethanol concentrations. A total of 50 μM S protein in the calorimetric cell was titrated with 700−800 μM mutant S-pep in buffer containing various concentrations of organic solvents in a VP isothermal titration calorimeter from Micro Cal Inc. (Northhampton, MA) at 25 °C. The titrations were performed as described previously (*23*, *24*). Data were analyzed using the ORIGIN software package and fitted to a single set of identical binding sites (*22*). The association constant for the 8Anb binding to S protein was low, and the titrations with this mutant were performed at 5 °C. The thermodynamic parameters thus obtained were extrapolated to 25 °C as described previously (*24*) for comparison with the other mutants. The extrapolation used the measured values of $\Delta G°$ and $\Delta H°$ at 5 °C and assumed that the $\Delta\Delta C_p$ of mutation was zero. The ΔC_p value of the WT as a function of methanol was determined by carrying out titrations at several different temperatures in the range of 5−25 °C (*24*) at each methanol concentration.

Crystallization, Data Collection, and Refinement. Purified S protein at a concentration of 1.0 mg/mL in water was mixed on ice with mutant S-pep (13Nva, 8Anb, or 8Nva) in the ratio of 3 mol of peptide/mol of S protein. The mixture was speedvacced to dryness and immediately redissolved in 6.0 M CsCl solution in 0.1 M sodium acetate buffer (pH 5.75 for 8Anb and 8Nva or pH 5.2 for 13Nva). An equal volume of 70% ammonium sulfate solution in the same buffer was added to it, and 8.0 μL drops were placed in the wells of 96-well flat-bottomed ELISA plates, covered and sealed with cover slips, and kept undisturbed at 20 °C. Crystals suitable for data collection were obtained in 5−7 days with final protein concentrations of 10 mg/mL in the drop for all three mutants. Crystals were transferred from the drops to Petri plates, and CsCl was washed off with repeated changes of a large excess of 70% ammonium sulfate

solution in 0.1 M sodium acetate at pH 4.75. Crystals were stored in this stabilization buffer for a few days.

Crystals were mounted in 0.7 mm capillary tubes, and diffraction data were collected using a MAR300 imaging plate system mounted on a Rigaku RU-200 rotating anode X-ray generator at room temperature. The crystal−plate distance was 100 mm, and images were collected for every 1° oscillation with an exposure time of 300 s. The data were processed using DENZO and scaled using SCALEPACK from the HKL program package (*26*).

The structures of the mutants were solved using the coordinates of WT as a starting model (PDB code 2RLN). The structure was refined using CNS version 1.1 (*27*), and further manual adjustments were made using O. Refinement included positional refinement followed by simulated annealing and finally *B*-factor refinement. Standard topology and parameter files in CNS were modified to include the nonnatural amino acid residues, Anb, Nva, and Nle. Water molecules were added using the water_pick program in CNS. $2f_o - f_c$ and $f_o - f_c$ maps were generated in CNS and contoured at 1.5σ and 3.0σ, respectively. Alternate conformations for the 13Nva side chain were modeled using CNS and O.

Cavity Volume and Solvent Accessibility Calculations. Cavities for the 8Anb, 8Nva, and 13Nva mutants were detected, and their volumes were calculated using the MC procedure previously described (*28*). The output of the program gives the centroids of the cavities in the protein molecule. The centroids of the side chains of Nle13, Phe8, and Phe120 were calculated using the coordinates of the WT (PDB code 2RLN). The volumes of all cavities whose centroids are within 6.0 Å of these side-chain centroids were summed to get the total cavity volume. ΔCav, the difference in cavity volume between mutants and WT is given by cavity volume (mutant) − cavity volume (WT). Cavities in the region of the side chain of Phe120 were also considered because there is a movement of this side chain in the 8Anb mutant. Solvent-accessible surface areas and solvent accessibility were calculated using the Lee and Richards (*29*) algorithm with a probe radius of 1.4 Å.

RESULTS

Crystallographic Structure of the Mutants. Structures for WT, 13Anb, and 8Nle have been described previously (*13*, *15*, *22*). A summary of the X-ray crystallographic data for the three RNase-S mutants determined in this study is shown in Table 1. All mutants were crystallized in the same space group, $P3_121$, with similar unit-cell parameters. A comparison of these structures with each other and with the WT reveal that the overall structure is similar in all of them. The backbone traces superpose well on each other. The root-mean-square deviation (rmsd) values for all backbone atoms with respect to that of the WT are 0.47, 0.29, and 0.28 Å for the 8Anb, 8Nva, and 13Nva mutants, respectively. The side-chain dihedral angles of residues that differ from the WT are listed in Table 2. The side chains that show significant differences from WT are Phe120 in 8Anb, Nle13 in both 8Anb and 8Nva, and Nva13 in 13Nva. The Leu51 side chain in 8Anb and 8Nva also differs significantly from the WT. The total cavity volumes around the side chains of residues 8, 13, and 120 were determined from the crystal structures and are listed in Table 3. In the absence of any structural rearrangement, deletion of a single methylene group from a side chain would be expected to result in a cavity with a cavity volume equal to the Voronoi volume of a buried methylene group [25 Å^3 (*30*)]. The expected values of ΔCav were calculated for each mutant and compared with the observed ones. The data show that the 8Anb mutant has a smaller cavity than expected for a Phe to Anb substitution. This is because the potential cavity created by the substitution is partly filled by the inward movement of the Phe120 side chain into this cavity (parts a and b of Figure 1). Such a movement has been previously observed for the F8A mutant also (*15*). The side chain of Nle13 also moves toward the created cavity. A similar movement is also seen in the 8Nva structure, but there is only a small change in conformation of Phe120 in this case. The Nva side chain in 13Nva exhibits

Table 1: Summary of Data Collection, Reduction, and Refinement for the RNase-S Mutants[a]

parameter	8Anb	8Nva	13Nva
$a = b$ (Å)	44.46	44.39	44.38
c (Å)	97.47	97.70	97.46
R_{merge} (%)	7.1	10.6	6.7
total number of reflections	125 966	91 284	103 336
number of unique reflections	10 679	7993	7872
resolution (Å)	1.8	2.0	2.0
completeness (%)	97.8	99.7	97.1
number of water molecules	63	55	53
R	19.66	19.55	18.84
R_{free}	22.63	25.01	23.50
rmsd bonds (Å)	0.0044	0.0046	0.0047
rmsd angles (deg)	1.20	1.19	1.17
backbone rmsd relative to the WT (Å)	0.47	0.29	0.28

[a] All mutants crystallized in the space group $P3_121$.

Table 2: Side-Chain Dihedral Angles of Residues Close to the Site of Mutation that Show Differences from the WT in at Least One Mutant Structure

residue	property	WT	8Anb	8Nva	13Nva
residue 8	χ_1	177	−178	−177	177
	χ_2	85		−180	84
residue 13	χ_1	−69	−57	−58	177[a], −49[b]
	χ_2	−60	179	180	−61[a], −55[b]
	χ_3	−53	−175	−177	
Leu51	χ_1	−178	−151	−161	175
	χ_2	50.3	−177	94.4[c]	59
Phe120	χ_1	−163	−87[c]	−161	−165
	χ_2	88	61[c]	69	88

[a,b] Values for the two alternate conformations. [c] Rotamers not typically found in proteins.

Table 3: Expected and Observed Change in Cavity Volumes of RNase-S Mutants with Respect to the WT and the Relative Distribution of the Change in Cavity Volumes around Residues 8, 13, and 120

mutant	expected Δ cavity volume (Å^3)[a]	observed Δ cavity volume (Å^3)	Δ cavity volume around residue 8	13	120
8Anb	77	37	13	−9	33
8Nva	52	49	62	−18	5
13Nva	25	22	2	15	5
8Nle[b]	27	33	27	0	6
13Anb[c]	50	50	18	33	−1

[a] Calculated based on the known average Voronoi volume of a buried CH_2 group of 25 Å^3 (*30*). [b] Calculated from PDB file 1D5E (*15*). [c] Calculated from PDB file 1RBD (*24*).

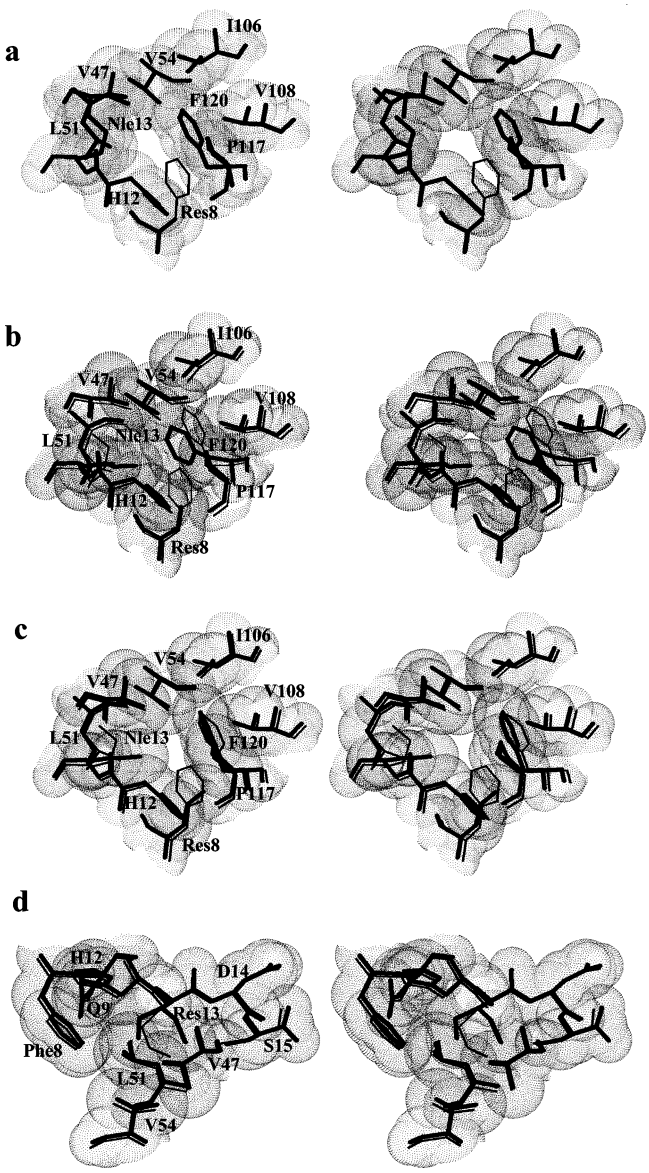

FIGURE 1: Stereo plots of the RNase-S structures (thick line) superposed on the WT (thin line) in the region around the mutation site. The van der Waals dot surface of residues around the cavity is shown for the mutant structures to highlight the cavity formed. (a) Model of the 8Anb mutant, constructed from the coordinates of the WT by mutating the Phe8 to Anb, superposed on the WT structure to show the potential cavity. (b) Actual structure of the 8Anb mutant showing the movement of the Phe120 side chain, which minimizes the potential cavity. (c) Structure of the 8Nva mutant superposed on the WT. (d) Structure of the 13Nva mutant superposed on the WT.

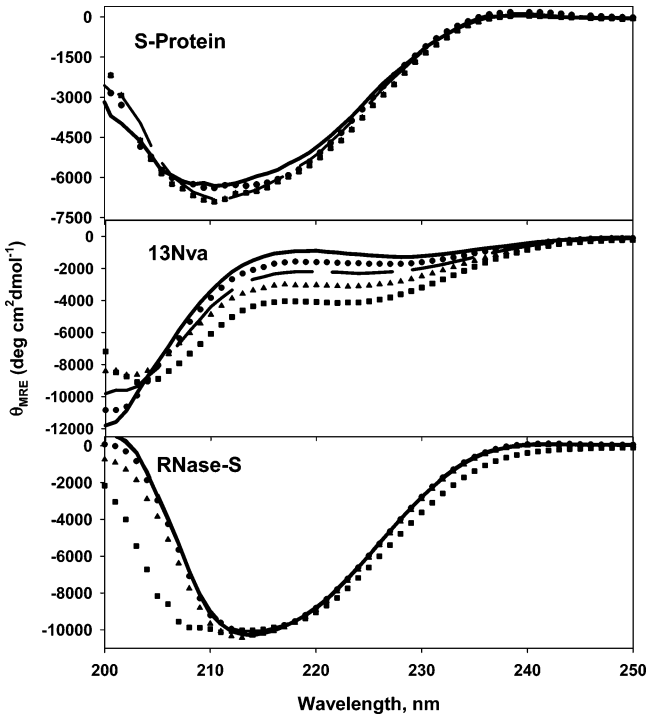

FIGURE 2: Far-UV CD spectra of S protein, a representative mutant S-pep (13Nva) and RNase S (with 13Nva) at room temperature in the presence of different concentrations of methanol. (—) represent spectra in the absence of methanol, while (●, - - -, ▲, and ■) represent spectra in the presence of 10, 20, 30, and 40% methanol, respectively.

alternate conformations. The observed cavity volume at this site is close to the expected value for this substitution. No water molecules were detected in any of the cavities in any of the three mutants.

Structural Studies as a Function of the Alcohol Concentration. CD spectra and activity measurements of RNase-S were carried out as a function of the alcohol concentration. The CD spectra of RNase-S were independent of the alcohol concentration in the range of 0−40% (Figure 2). The effect of methanol on the CD spectra of the S protein and the free 13Nva peptide were also examined (Figure 2). While the CD spectra of S protein remained the same at all methanol concentrations examined, the spectra were a little different for the free 13Nva peptide. This showed a small increase in helicity from 1.7% in the absence of methanol to 7.1% in the presence of 40% methanol. The helicities were calculated assuming that 100% helix has an ellipticity of 29 200° cm^2 dmol^{-1} (*31*). Residues 8 and 13 are part of the N-terminal helix that extends from residues 3 to 13 in RNase-S (or RNase-A). Solvent accessibilities of these two residues were calculated using the coordinates of only the S-pep region in the absence of S protein, and we found them to be about 75 and 55%, respectively, in all of the RNase-A and RNase-S structures examined [WT (2RLN), 7RSA, and 1RNY]. Hence, it can be assumed that both residues 8 and 13 of the free S-pep are highly accessible to the solvent even in the presence of 40% methanol. RNase-S activity was similarly unaffected by alcohol at concentrations up to 40% (data not shown). Crystal structures of RNase-A have been previously determined in the presence and absence of alcohol. The coordinates for RNase-A crystallized from 43% tertiary butyl alcohol (7RSA) (*32*) and from 80% ammonium sulfate/3.0 M cesium chloride (1RNY) (*33*) were compared. The structures are virtually identical (rmsd = 0.42 Å). The volume of the cavity close to Met 13 in RNase-A was calculated using the MC procedure as described previously (*28*). The cavity volume was also virtually identical in both structures (86 and 92 Å^3 for 7RSA and 1RNY, respectively). Hence, it is reasonable to assume that the cavity volumes of the various mutants are also independent of the alcohol concentration.

Thermodynamics of Interaction of S Protein with Mutant S-pep's. The thermodynamics of the interaction of S protein with the WT and mutant S-pep's in the absence and presence of different concentrations of methanol and ethanol were

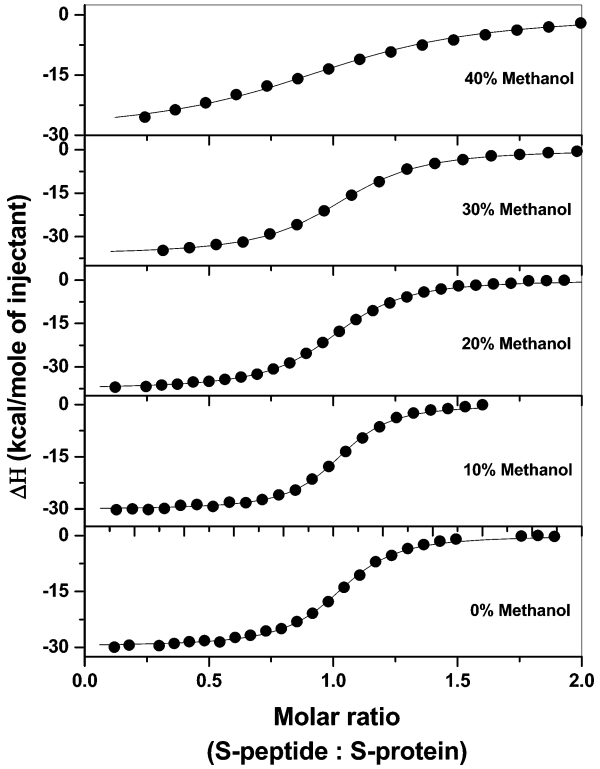

FIGURE 3: Titration profiles for the WT peptide with S protein in acetate buffer containing varying concentrations of methanol at 20 °C. The enthalpy change per mole of peptide injected is plotted as a function of the molar ratio of mutant S-pep/S protein.

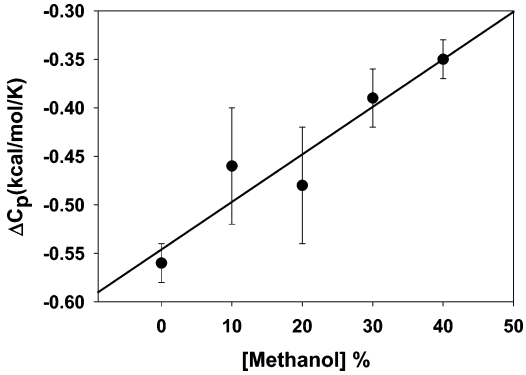

FIGURE 4: ΔC_p as a function of the methanol concentration for the binding of WT to S protein.

studied using ITC. The thermodynamic parameters for the association of the WT, as well as each mutant S-pep analogue, with S protein in the absence and presence of different concentrations of methanol and ethanol at 25 °C were determined (Tables 1−7 in the Supporting Information). Figure 3 shows the titration profiles (enthalpy change as kcal/mol of peptide injected, as a function of the molar ratio of peptide/protein) for the WT at 20 °C in the presence of varying concentrations of methanol. The WT peptide was titrated with S protein over the temperature range of 5−25 °C at each concentration of methanol to obtain ΔC_p as a function of methanol (Figure 4). The magnitude of ΔC_p decreases linearly with an increasing methanol concentration, with the values being -0.56 ± 0.02, -0.46 ± 0.06, -0.48 ± 0.06, -0.39 ± 0.03, and -0.35 ± 0.02 kcal mol^{-1} K^{-1} in the presence of 0, 10, 20, 30, and 40% methanol, respectively. Over the 0−40% range of methanol examined, ΔC_p decreases by 38%, suggesting a similar decrease in the magnitude of the hydrophobic driving force over this range of methanol concentrations.

Table 4: Difference Thermodynamic Parameters for the Interaction of S-pep Analogues with S Protein Relative to the WT as a Function of the Methanol Concentration at 25 °C

peptide	buffer	percent methanol	$\Delta\Delta H°$ (kcal/mol)	$T\Delta\Delta S$ (kcal/mol)	$\Delta\Delta G°$ (kcal/mol)
13Anb	acetate	0	1.5 ± 1.1	0.9 ± 1.2	0.6 ± 0.03
	pH 6.0	10	0.2 ± 0.7	-0.6 ± 0.8	0.7 ± 0.04
		20	0.8 ± 1.1	0.2 ± 0.5	0.6 ± 0.05
		30	1.6 ± 0.6	1.1 ± 0.7	0.6 ± 0.05
13Nva	acetate	0	0.4 ± 0.9	0.5 ± 1.0	-0.1 ± 0.03
	pH 6.0	10	-0.1 ± 0.5	-0.2 ± 0.6	0.1 ± 0.04
		20	4.4 ± 1.2	4.5 ± 1.2	-0.1 ± 0.0
		30	6.8 ± 0.6	6.9 ± 0.6	0.0 ± 0.05
8Anb	phosphate	0	10.8 ± 1.1	6.6 ± 1.2	4.3 ± 0.05
	pH 7.0	10	3.1 ± 1.7	-1.4 ± 1.7	4.6 ± 0.10
		20	-14.1 ± 3.2	-18.9 ± 3.2	4.8 ± 0.24
8Nle	phosphate	0	1.6 ± 2.3	-0.7 ± 2.3	2.3 ± 0.1
	pH 7.0	10	8.5 ± 1.9	6.5 ± 3.5	2.1 ± 0.06
		20	7.3 ± 0.5	5.4 ± 0.6	1.9 ± 0.14
		30	7.8 ± 1.0	5.7 ± 1.1	2.1 ± 0.07
8Nva	phosphate	0	2.4 ± 1.4	0.2 ± 1.4	2.3 ± 0.1
	pH 7.0	10	3.1 ± 1.8	1.0 ± 3.4	2.1 ± 0.1
		20	13.9 ± 4.0	11.5 ± 3.9	2.5 ± 0.2

Table 5: Difference Thermodynamic Parameters for the Interaction of S-pep Analogues with S Protein Relative to the WT as a Function of the Ethanol Concentration at 25°C

peptide	buffer	percent ethanol	$\Delta\Delta H°$ (kcal/mol)	$T\Delta\Delta S$ (kcal/mol)	$\Delta\Delta G°$ (kcal/mol)
13Anb	acetate	0	1.5 ± 1.1	0.9 ± 1.2	0.6 ± 0.03
	pH 6.0	10	-0.8 ± 1.4	-1.4 ± 1.4	0.7 ± 0.05
		20	-0.2 ± 0.6	-0.6 ± 0.7	0.4 ± 0.02
		30	0.5 ± 0.9	-0.4 ± 0.9	0.7 ± 0.2
13Nva	acetate	0	0.4 ± 0.9	0.5 ± 1.0	-0.1 ± 0.03
	pH 6.0	10	-0.1 ± 1.1	-0.2 ± 1.1	0.2 ± 0.02
		20	0.9 ± 0.6	1.0 ± 0.7	0.0 ± 0.01
		30	-0.5 ± 0.6	-0.7 ± 0.6	0.1 ± 0.2
8Nle	phosphate	0	1.6 ± 2.3	-0.7 ± 2.3	2.3 ± 0.1
	pH 7.0	10	1.4 ± 1.4	-0.9 ± 1.5	2.3 ± 0.04
		20	1.5 ± 0.4	-0.7 ± 0.4	2.2 ± 0.06
8Nva	phosphate	0	2.5 ± 1.4	0.2 ± 1.4	2.3 ± 0.1
	pH 7.0	10	2.7 ± 1.6	0.4 ± 1.6	2.3 ± 0.02
		20	20.4 ± 0.5	18.3 ± 0.5	2.1 ± 0.05

Tables 4 and 5 list the changes in thermodynamic parameters for the interactions of the mutants with S protein relative to the WT. It can be seen that for all of the mutants the $\Delta\Delta G°$ values do not significantly differ in the presence of different concentrations of methanol or ethanol. Because decreasing the hydrophobic driving force by the presence of organic solvents does not significantly affect the free-energy changes, it implies that a reduced hydrophobic driving force does not play a major part in the destabilization of these mutants. The difference in thermodynamic binding parameters for each peptide between the values in ethanol and methanol, respectively, was also analyzed. As expected, binding is typically weaker with the more hydrophobic ethanol additive, resulting in positive values of $\Delta\Delta G°$ of about 0.2−0.6 kcal/mol. The positive value of $\Delta\Delta G°$ is due to a negative value of $T\Delta\Delta S$, consistent with an entropy-driven hydrophobic driving force under these conditions.

Substitution of Phe8 and Nle13 by smaller residues destabilizes the complex as indicated from the positive values

of $\Delta\Delta G°$. Because the hydrophobic driving force is not the major contributor to the relative stability of these mutants, the difference in free energy upon such large to small substitutions must arise from the loss in packing interactions as reported earlier (*15*).

DISCUSSION

Quantitative estimates of the strength of the hydrophobic driving force are primarily derived from measurements of the thermodynamics of transfer of small, relatively nonpolar solutes from either the liquid, solid, or gas phase into an aqueous solution (*2*−*7*). These yield a value of about 25−30 cal mol^{-1} Å^{-2} for the hydrophobic driving force. For transfer of small nonpolar solutes from the aqueous phase to the nonpolar phase (analogous to a protein-folding reaction), at room temperature, values of $\Delta H_{tr}°$ are close to zero, while values of ΔS_{tr} are positive (*15*), (*4*). With a decrease in size of the solute, values of $\Delta\Delta H_{tr}°$ are close to zero but values of $\Delta\Delta S_{tr}$ are always large and negative and result in a positive value of $\Delta\Delta G_{tr}°$ for a small nonpolar solute relative to a larger one (Table 4 of ref *15*). Some recent simulations and calculations (*34*−*36*) have suggested that the nature of hydrophobic hydration depends strongly on the size and topography of the solute. Locally convex hydrophobic patches are thought to be characterized by clathrate-like solvent structures, similar to those believed to be formed around small, spherical nonpolar solutes. However, flat and extended hydrophobic surfaces may be associated with a less ordered and inverted clathrate solvent with disrupted hydrogen bonding for water close to the solute. The former, clathrate type of association will be associated with a reduced solvent entropy, and hence, the hydrophobic effect will be entropy-driven with positive value of $\Delta S_{tr}°$ from water to nonpolar media. In contrast, for the larger and flatter hydrophobic solutes, it is likely that the hydrophobic effect will be enthalpically driven.

As discussed in an earlier section, thermodynamic studies of large to small substitutions in globular proteins have been used to estimate the strength of the hydrophobic driving force in protein folding. Some of these studies yielded an estimate of as high as 47 cal mol^{-1} Å^{-2} (*37*−*39*). However, it was subsequently shown that this large number was due to neglect of the contribution of cavity formation to the measured decrease in stability (*28*). The latter analysis yielded an estimate of the hydrophobic driving force of at most 18.5 cal mol^{-1} Å^{-2}. On average, deletion of a single methylene group in a well-packed structure was predicted to result in losses in stability of 0.41 and 0.7 kcal mol^{-1}, resulting from decreases in hydrophobicity and packing, respectively.

The large contribution of loss of packing interactions to the observed stability decrease was also consistent with positive values of $\Delta\Delta H°$ and $\Delta\Delta S$ of folding for such mutants (*15*). Positive values of $\Delta\Delta H°$ and $\Delta\Delta S$ are the opposite of what is experimentally observed in small molecule transfer studies, discussed above. In the present work, we have adopted an alternative approach to determine the relative contributions of close packing and the hydrophobic effect to destabilization of mutants with large to small substitutions. Stability measurements in WT and mutant proteins have been carried out in the presence of varying concentrations of methanol and ethanol. These two additives

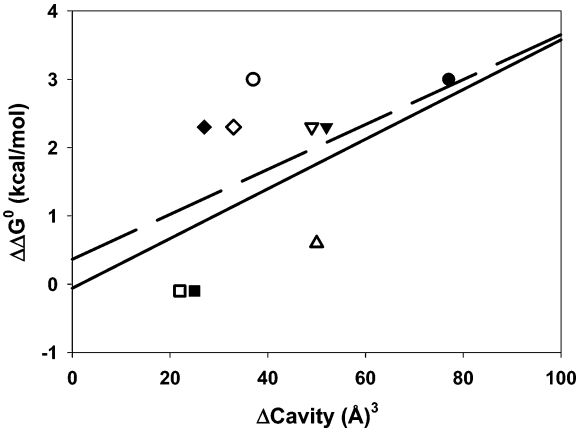

FIGURE 5: $\Delta\Delta G°$ as a function of expected (●, ▼, ◆, ▲, and ■) and observed (○, ▽, ◇, △ and, □) cavity volumes for the 8Anb (●, ○), 8Nva (▼, ▽), 8Nle (◆, ◇), 13Anb (▲, △), and 13Nva (■, □) mutants. (—) and (- - -) represent the linear fits of the data for the expected and observed cavity volumes, respectively, and have correlation coefficients of 0.59 and 0.29, respectively.

will decrease the hydrophobic driving force. Hence, if the destabilization of mutants with large to small substitutions is primarily due to the hydrophobic effect, it is expected that the magnitude of $\Delta\Delta G°$ [$\Delta G°$(mutant) − $\Delta G°$(wild type)] will decrease with an increase in the alcohol concentration. Furthermore, this decrease should be larger for the more nonpolar ethanol additive. The data in Tables 4 and 5 clearly show that values of $\Delta\Delta G°$ are virtually independent of the methanol or ethanol concentration. This confirms our earlier assertion (*15*, *28*) that loss of packing interactions rather than the hydrophobic effect is the main determinant of the observed destabilization. In Figure 5, the observed value of $\Delta\Delta G°$ is plotted against the observed cavity volume as well as against the expected cavity volume (assuming no structural rearrangement) for RNase-S mutants characterized in both this as well as an earlier study (*15*). Only those mutants with unbranched substitutions at positions 8 and 13 were considered. There is a better correlation between $\Delta\Delta G°$ and the expected ΔCav ($R = 0.59$) than with the observed ΔCav ($R = 0.29$). This probably arises from the fact that protein rearrangement associated with reduction in cavity volume (relative to the expected ΔCav) is associated with an energetic cost. Evidence for this comes from the observation that side chains that undergo movement to fill in the cavity sometimes have unfavorable dihedral angles (see χ_1 and χ_2 for Phe120 in the 8Anb structure and χ_2 for Leu51 in the 8Nva structure, Table 2; these dihedral angles are not typically found in proteins). Similar observations were previously made for other mutants at position 13 in RNase-S (*13*). To interpret the values of $\Delta\Delta G°$ as a function of the alcohol concentration, it is important to confirm that the structure of the protein and the volume of the internal cavity are not affected by alcohol. As discussed in the results section, CD, activity, and previous crystallographic studies all suggest that the structures of S-pep, S protein, and RNase S are not affected by alcohol over the concentration ranges studied.

To estimate the approximate reduction in the strength of the hydrophobic driving force as a function of the alcohol concentration, two different approaches were taken. First, the previously reported dependence of the surface tension on the alcohol concentration (*40*) was examined (Figure 6).

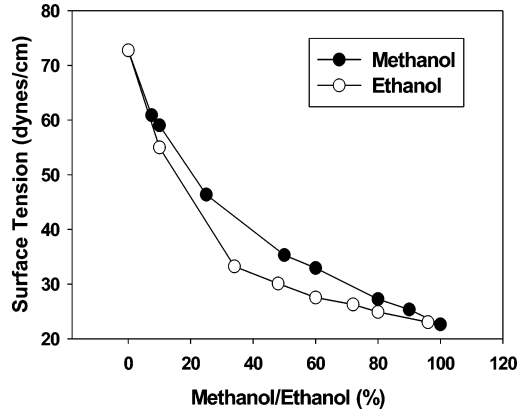

FIGURE 6: Surface tension of the aqueous solution of methanol (●) and ethanol (○) as a function of the methanol and ethanol concentration (%, v/v) at 20 °C (*40*).

The surface tension of water decreases from about 72 dynes/cm (in the absence of alcohol) to about 35 dynes/cm in 50% methanol and to about 30 dynes/cm in 50% ethanol. Second, the dependence of ΔC_p of binding of WT peptide to S protein on the alcohol concentration was measured (Figure 4). Here too, there was a linear decrease of approximately 38% from -0.56 kcal mol^{-1} K^{-1} in the absence of alcohol to -0.35 kcal mol^{-1} K^{-1} at 40% methanol. Both of these approaches are consistent with a decrease in the magnitude of the hydrophobic driving force to about 60−70% of its aqueous solution value over the range of alcohol concentrations studied. Despite this significant decrease, there is no detectable change in values of $\Delta\Delta G°$ with the alcohol concentration (Tables 4 and 5). When all of the data are taken together, they strongly suggest that the reduced stability of mutants with large to small substitutions is primarily due to the loss of packing interactions rather than a reduced hydrophobic driving force. We had previously estimated the strength of the hydrophobic driving force to have an upper limit of about 18 cal mol^{-1} Å^{-2} corresponding to about 0.41 kcal mol^{-1} per methylene group deleted. In the mutants studied here, the number of carbon atoms deleted varies from 1 (Nle → Nva) to 4 (Phe → Nva). This would correspond to stability decreases of 0.4−1.6 kcal mol^{-1} because of a reduced hydrophobic driving force. A reduction of about 30% in the hydrophobic driving force should lead to decreases of between 0.1 and 0.5 kcal/mol in values of $\Delta\Delta G°$ as a function of the alcohol concentration. The estimated standard error in $\Delta\Delta G°$ is typically less than 0.1 kcal mol^{-1} (Tables 4 and 5). The fact that there is no observable decrease in $\Delta\Delta G°$ suggests that the true value of the hydrophobic driving force is somewhat lower than 18 cal mol^{-1} Å^{-2} for protein folding.

ACKNOWLEDGMENT

Dr. B. Gopal and K. Saikrishnan are acknowledged for their help in crystal structure determination of the mutants. We thank Kausik Chakraborty for his help with cavity volume calculations.

SUPPORTING INFORMATION AVAILABLE

Tables 1−7 expressing thermodynamic parameters. This material is available free of charge via the Internet at http://pubs.acs.org.

REFERENCES

1. Dill, K. A. (1990) Dominant forces in protein folding, *Biochemistry 29*, 7133−7155.
2. Murphy, K. P., Privalov, P. L., and Gill, S. J. (1990) Common features of protein unfolding and dissolution of hydrophobic compounds, *Science 247*, 559−561.
3. Murphy, K. P., and Gill, S. J. (1991) Solid model compounds and the thermodynamics of protein unfolding, *J. Mol. Biol. 222*, 699−709.
4. Privalov, P. L., and Gill, S. J. (1988) Stability of protein structure and hydrophobic interaction, *Adv. Protein Chem. 39*, 191−234.
5. Chothia, C. (1974) Hydrophobic bonding and accessible surface area in proteins, *Nature 248*, 338−339.
6. Richards, F. M. (1977) Areas, volumes, packing and protein structure, *Annu. Rev. Biophys. Bioeng. 6*, 151−176.
7. Tanford, C. (1980) *The Hydrophobic Effect*, Wiley, New York.
8. Pace, C. N. (1992) Contribution of the hydrophobic effect to globular protein stability, *J. Mol. Biol. 226*, 29−35.
9. Sturtevant, J. (1994) The thermodynamic effects of protein mutations, *Curr. Opin. Struct. Biol. 4*, 69−78.
10. Matthews, B. W. (1995) Studies on protein stability with T4 lysozyme, *Adv. Protein Chem. 46*, 249−278.
11. Eriksson, A. E., Baase, W. A., Zhang, X. J., Heinz, D. W., Blaber, M., Baldwin, E. P., and Matthews, B. W. (1992) Response of a protein structure to cavity-creating mutations and its relation to the hydrophobic effect, *Science 255*, 178−183.
12. Varadarajan, R., Richards, F. M., and Connelly, P. R. (1990) Proteins: The hard sphere, structure, and energetics, *Curr. Sci. 59*, 819−824.
13. Varadarajan, R., and Richards, F. M. (1992) Crystallographic structures of ribonuclease S variants with nonpolar substitution at position 13: Packing and cavities, *Biochemistry 31*, 12315−12327.
14. Richards, F. M., and Lim, W. A. (1993) An analysis of packing in the protein folding problem, *Q. Rev. Biophys. 26*, 423−498.
15. Ratnaparkhi, G. S., and Varadarajan, R. (2000) Thermodynamic and structural studies of cavity formation in proteins suggest that loss of packing interactions rather than the hydrophobic effect dominates the observed energetics, *Biochemistry 39*, 12365−12374.
16. Richards, F. M., and Vithayathil, P. J. (1959) The preparation of subtilisn-modified ribonuclease and the separation of the peptide and protein components, *J. Biol. Chem. 234*, 1459−1465.
17. Richards, F. M., and Wyckoff, H. W. (1971) Bovine pancreatic ribonuclease, *Enzymes 4*, 647−806.
18. Wyckoff, H. W., Tsernoglou, D., Hanson, A. W., Knox, J. R., Lee, B., and Richards, F. M. (1970) The three-dimensional structure of ribonuclease-S. Interpretation of an electron density map at a nominal resolution of 2 Å, *J. Biol. Chem. 245*, 305−328.
19. Kim, E. E., Varadarajan, R., Wyckoff, H. W., and Richards, F. M. (1992) Refinement of the crystal structure of ribonuclease S. Comparison with and between the various ribonuclease A structures, *Biochemistry 31*, 12304−12314.
20. Taylor, H. C., Richardson, D. C., Richardson, J. S., Wlodawer, A., Komoriya, A., and Chaikes, I. M. (1981) "Active" conformation of an inactive semi-synthetic ribonuclease-S, *J. Mol. Biol. 149*, 313−317.
21. Hearn, R. P., Richards, F. M., Sturtevant, J. M., and Watt, G. D. (1971) Thermodynamics of the binding of S-peptide to S-protein to form ribonuclease S, *Biochemistry 10*, 806−817.
22. Thomson, J., Ratnaparkhi, G. S., Varadarajan, R., Sturtevant, J. M., and Richards, F. M. (1994) Thermodynamic and structural consequences of changing a sulfur atom to a methylene group in the M13Nle mutation in ribonuclease-S, *Biochemistry 33*, 8587−8593.
23. Connelly, P. R., Varadarajan, R., Sturtevant, J. M., and Richards, F. M. (1990) Thermodynamics of protein−peptide interactions in the ribonuclease S system studied by titration calorimetry, *Biochemistry 29*, 6108−6114.
24. Varadarajan, R., Connelly, P. R., Sturtevant, J. M., and Richards, F. M. (1992) Heat capacity changes for protein−peptide interactions in the ribonuclease S system, *Biochemistry 31*, 1421−1426.
25. Neumann, U., and Hofsteenge, J. (1994) Interaction of semisynthetic variants of RNase A with ribonuclease inhibitor, *Protein Sci. 3*, 248−256.

26. Otwinowski, Z., and Minor, W. (1997) Processing of X-ray diffraction data collected in oscillation mode, *Methods Enzymol. 276*, 307−326.
27. Brunger, A. T., Adams, P. D., Clore, G. M., DeLano, W. L., Gros, P., Grosse-Kunstleve, R. W., Jiang, J. S., Kuszewski, J., Nilges, M., Pannu, N. S., Read, R. J., Rice, L. M., Simonson, T., and Warren, G. L. (1998) Crystallography and NMR system: A new software suite for macromolecular structure determination, *Acta. Crystallogr., Sect. D 54*, 905−921.
28. Chakravarty, S., Bhinge, A., and Varadarajan, R. (2002) A procedure for detection and quantitation of cavity volumes proteins. Application to measure the strength of the hydrophobic driving force in protein folding, *J. Biol. Chem. 277*, 31345−31353, Epub June 17, 2002.
29. Lee, B., and Richards, F. M. (1971) The interpretation of protein structures: Estimation of static accessibility, *J. Mol. Biol. 55*, 379−400.
30. Harpaz, Y., Gerstein, M., and Chothia, C. (1994) Volume changes on protein folding, *Structure 2*, 641−649.
31. Mitchinson, C., and Baldwin, R. L. (1986) The design and production of semisynthetic ribonucleases with increased thermostability by incorporation of S-peptide analogues with enhanced helical stability, *Proteins 1*, 23−33.
32. Wlodawer, A., Svensson, L. A., Sjolin, L., and Gilliland, G. L. (1988) Structure of phosphate-free ribonuclease A refined at 1.26 Å, *Biochemistry 27*, 2705−2717.
33. Fedorov, A. A., Joseph-McCarthy, D., Fedorov, E., Sirakova, D., Graf, I., and Almo, S. C. (1996) Ionic interactions in crystalline bovine pancreatic ribonuclease A, *Biochemistry 35*, 15962−15979.
34. Cheng, Y. K., and Rossky, P. J. (1998) Surface topography dependence of biomolecular hydrophobic hydration, *Nature 392*, 696−699.
35. Lum, K., Chandler, D., and Weeks, J. D. (1999) Hydrophobicity at small and large length scales, *J. Phys. Chem. B 103*, 4570−4577.
36. Cheng, Y. K., Sheu, W. S., and Rossky, P. J. (1999) Hydrophobic hydration of amphipathic peptides, *Biophys. J. 76*, 1734−1743.
37. Nicholls, A., Sharp, K. A., and Honig, B. (1991) Protein folding and association: Insights from the interfacial and thermodynamic properties of hydrocarbons, *Proteins 11*, 281−296.
38. Sharp, K. A., Nicholls, A., Friedman, R., and Honig, B. (1991) Extracting hydrophobic free energies from experimental data: Relationship to protein folding and theoretical models, *Biochemistry 30*, 9686−9697.
39. Sharp, K. A., Nicholls, A., Fine, R. F., and Honig, B. (1991) Reconciling the magnitude of the microscopic and macroscopic hydrophobic effects, *Science 252*, 106−109.
40. Lide, D. R. (1995) CRC Press, Boca Baton, FL.

BI050001+